ENGINEERING JOURNAL

*Article*

# Coseismic and Postseismic Displacement of 2011 $M_w$ 6.8 Tarlay Earthquake, Myanmar using InSAR Techniques and Inversion Analysis

**Pattama Phodee**[1,a,*], **Itthi Trisirisatayawong**[1,b], **and Anuphao Aobpaet**[2,c]

1 Department of Survey Engineering, Faculty of Engineering, Chulalongkorn University, Bangkok 10330, Thailand
2 Geo-Informatics and Space Technology Development Agency (Public Organization), Bangkok 10210, Thailand
E-mail: [a]pattamaphodee@yahoo.com (Corresponding author), [b]itthi.t@eng.chula.ac.th, [c]anuphao@gistda.or.th

**Abstract.** In this study, we investigate the March 24th, 2011 $M_w$=6.8 Tarlay earthquake, Myanmar using InSAR and inversion analysis. We firstly invert InSAR coseismic displacement from our previous study. The inversions for fault parameters are carried out in both Single and Multi-patch model. The coseismic slip of 2.5 meters from Single-patch solution is then combined with long-term slip rate from geomorphological study, resulting in an estimate of 1,040-4,160 years recurrence period. Then, coulomb stress changes on nearby faults in northern Thailand are calculated. It is found that stress in western and middle segments of Mae Chan fault decreases significantly while stress increase in eastern segment of Mae Chan, Mae Ing and Chiang Kham fault. Finally, the results from PSInSAR of 29 Radarsat-2 images reveal postseismic displacement rates between -24.4 to 34.5 millimeters per year.

**Keywords:** Tarlay earthquake, Nam Ma Fault, coseismic motion, postseismic motion, inversion, InSAR, Coulomb stress change.

**ENGINEERING JOURNAL** Volume 19 Issue 2
Received 16 July 2014
Accepted 1 December 2014
Published 30 April 2015
Online at http://www.engj.org/
DOI:10.4186/ej.2015.19.2.157

DOI:10.4186/ej.2015.19.2.157

## 1. Introduction

The $M_w$=6.8 Tarlay earthquake occurred in western part of Nam Ma fault, Myanmar, on March 24th, 2011. The hypocenter was located at 20.705N, 99.949E and the depth was approximately 10 kilometers below surface as estimated by USGS [1]. This is the ensuing strongest seismic event on SE-Asia peninsular since the 2004 $M_w$=9.2 Sumatra-Andaman earthquake [2] which caused the Indian Ocean tsunami and became one of the big catastrophic events in this century. Shake resulted from Tarlay earthquake was felt in Kunming, Hanoi and even Bangkok which are several hundred kilometers from the epicenter.

The Nam Ma fault, a NE-SW trending strike-slip fault, originates in southern China, extends as a narrow 215 kilometers long into northwest Laos and propagates into northern Myanmar [3] with a 12 kilometers left-lateral offset of the Mekong River channel at the central part of the fault [4]. Nam Ma Fault lies in about 60 kilometers north of another left-lateral in northern Thailand called Mae Chan fault [2]. These two left-lateral faults are farther to the southeast in the central Shan-Sino domain and the geology details can be found in [5]. The faults are members of a group of left-lateral faults in Shan fault system posing as network triangle faults between Sagaing fault in Myanmar and Red River fault in northern Vietnam. Many large earthquakes occurred in this fault system since late 20th century [6, 7] as shown in Fig. 1.

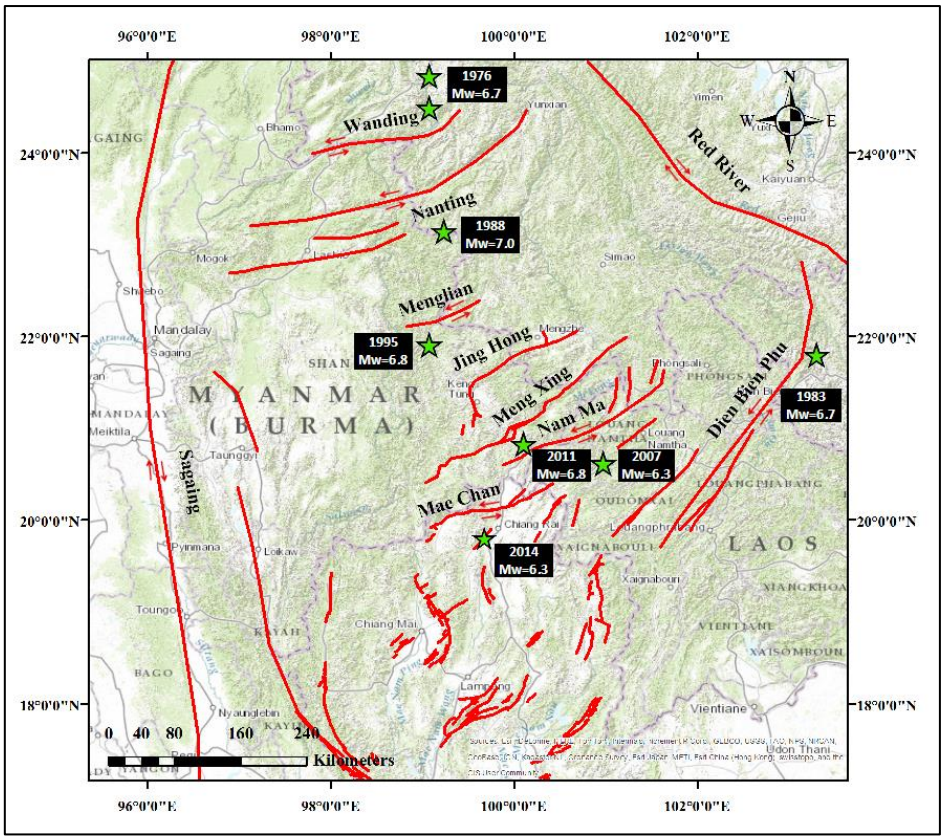


Fig. 1. Map of faults in Shan fault system. Green stars represent epicenters of large earthquake ($M_w$>6.3) events since 1976.

An important parameter of earthquake cycle model, which is summarized in Fig. 2, is recurrence period. The determination of coseismic slip is important because it is crucial in determining the recurrence period. The earthquake cycle can be divided into three phases. First, in the interseismic stage, a procedure of strain accumulation in the earth's crust in an opposite direction is shown in Fig. 2(b). Next, Fig. 2(c) shows a procedure of coseismic motion when the stress accumulation reaches a breaking point, and the energy is abruptly released resulting in an earthquake. After the seismic event, the stress will continue to be relaxed and caused deformation during a period called postseismic phase [8].

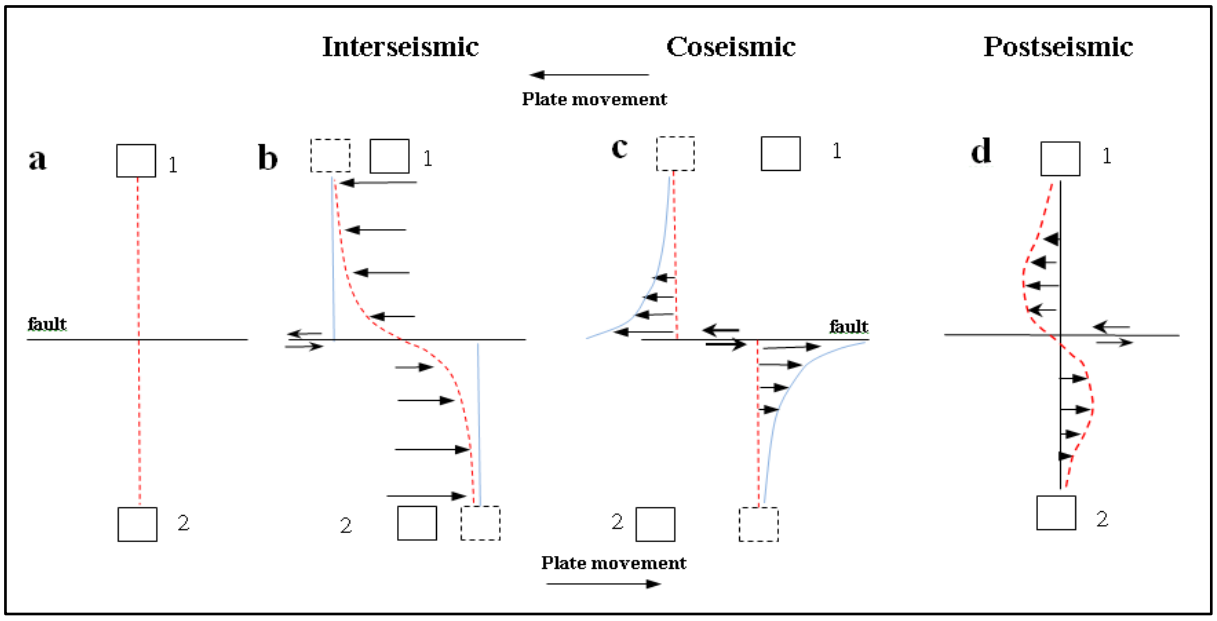


Fig. 2. Earthquake cycle as explained by Reid's elastic model in each seismic phase consists of interseismic, coseismic and postseismic. a) It reveals a fault plane which is located between two crusts. b) The black arrow represents the displacement of the exemplified left-lateral strike-slip fault, red-dashed has become curved due to accumulation of strain. c) coseismic strain release causing an earthquake. The earth's crusts slip in the opposite direction. The blue lines in c) indicate the sum of deformation before and after earthquake. d) The red dot illustrates stress release to postseismic. (modified from [8] and [9]).

InSAR has been proved to be a useful tool in a number of earthquake studies. Initial studies in the 1990s and early 2000s were carried out with 2-pass InSAR technique of C-band SAR images from ERS-1/2 and Envisat over arid or desert areas. Detail of the technique is now well covered and good introduction can be found elsewhere. A major limitation of C-band 2-pass InSAR is that in vegetated and tropical areas, the radar phase change of geophysical signal of interest is corrupted by larger phase change resulted from other causes such as growing/dying vegetation or atmospheric differences at the two acquisition time of radar images. This is known as decorrelation problem. L-band radar with longer wavelength has a better capability of penetration vegetation and so can maintain correlation much longer than C-band data. This leads to a number of recent earthquake studies in non-arid areas with ALOS PALSAR L-band images. The examples of applying ALOS PALSAR for coseismic deformation was the $M_w$=7.9, 12 May 2008 Wenchuan earthquake that struck the western Sichuan province (China) along the topographic escarpment between the Tibetan plateau and the Sichuan basin [10–13]. The results show strike-slip motion along 145 kilometers long Yingxiu–Beichuan fault and mainly thrust faulting along the sub-parallel, 105 kilometers long Beichuan–Qingchuan fault. In 2009, there was the first study case using X, C and L-band SAR data for the investigation of the same earthquake [14]. ALOS PALSAR, COSMO-SkyMed, Envisat data were acquired covering different temporal and spatial baselines in $M_w$=6.3 L'Aquila (Central Italy) earthquake event for the coseismic motion. The results from InSAR reveal the surface displacement pattern in a very useful detail. Later on in 2010, the $M_w$=7.1 Darfield (Canterbury) earthquake occurred in New Zealand which was followed by a sequence of large aftershocks including the $M_w$=6.3 Christchurch earthquake on February 21, 2011, [15]. In both events, the coseismic movements have been measured by ALOS PALSAR. The more details on Darfield earthquake which ruptured a complex set of strike-slip and secondary reverse faults can be found in [16].

We present in section 2, 3 and 4 our attempt to solve for Nam Ma fault parameters by inverting the coseismic displacement of Tarlay earthquake obtained from 2-pass InSAR of ALOS PALSAR images as reported in the previous study of [2]. The comparisons of along strike-slips from our model are then compared with filed data as described in section 5. We then calculate the distribution of Coulomb stress change for Mae Chan fault in northern Thailand. This is detailed in section 6. In section 7, we investigate postseismic motion of Tarlay earthquake using Time-series InSAR technique with a stack of 19 Radarsat-2 images. Section 8 concludes the paper.

DOI:10.4186/ej.2015.19.2.157

## 2. InSAR for Coseismic Deformation Detection

In the previous study of [2], 4 ALOS PALSAR Single Look Complex images in both ascending track 126 and descending track 486 orbits were acquired before and after earthquake. This is shown in the Table 1 below.

Table 1. Acquisition details of ALOS PALSAR data (fine beam mode with HH- polarization).

| Path | Master date | Slave date | Perpendicular Baseline (meter) | Temporal Baseline (day) |
|---|---|---|---|---|
| Ascending | 16 February 2011 | 3 April 2011 | 48.7 | 46 |
| Descending | 14 February 2011 | 1 April 2011 | 436.2 | 46 |

The mentioned study can be summarized as follows. The study employed 2-pass InSAR technique available in GAMMA software package to generate multi-looked interferogram of both ascending and descending image pairs (4 and 6 multilook in range and azimuth direction respectively). The coherence of both image pairs are very good even in the dense vegetation in the study area which is in tropical zone. Topographic phases were simulated from SRTM 90 meter (3 arc-second) elevation and removed from the interferograms. The differential interferograms of both paths, in radar coordinate systems, are presented in Fig. 3. The study then perform phase unwrapping with a minimum cost-flow algorithm of Delauney triangulation. After phase unwrapping, the results which still are in radar coordinates are geocoded into UTM (zone 47) coordinate system.

From Fig. 3, the results reveal displacement in line-of-sight direction (LOS). From the interferogram, a 1.2 meters left-lateral offset in the radar LOS can be estimated across the fault. Small offsets around 12 centimeters are observable at distance of more than 20 kilometers from the epicenter. The observed coseismic motions suggest that earthquake could also have impact on Mae Chan fault, around 50 kilometers to the south of the earthquake.

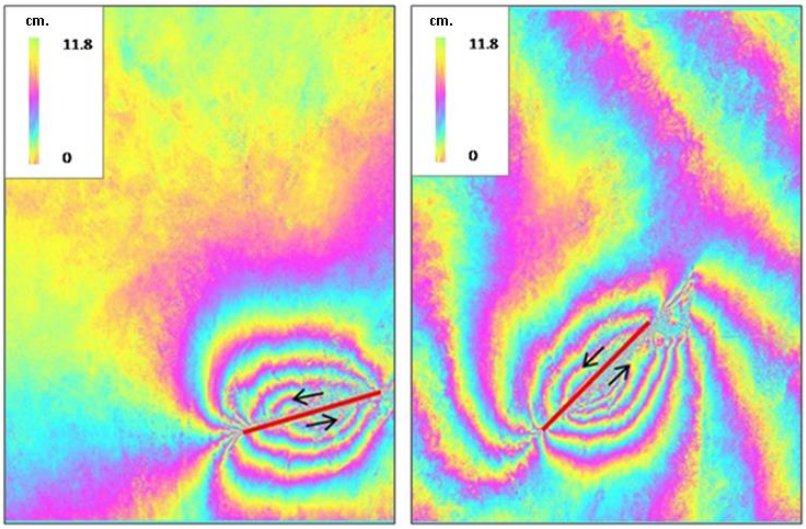


Fig. 3. Differntial interferograms formation using 2-pass InSAR from ascending (left) and descending path (right) [2], 1 color cycles=11.8 centimeters and red line is Nam Ma fault.

## 3. Inversion for Fault Geometry Parameters by Single-patch Model

The observed coseismic displacements from both ascending and descending data are employed in the estimation of fault parameters. We treat the surface displacements as the elastic response to a slip on a planar fault, assuming a model of vertically varying stiffness. The primary fault model (Okada 1985) contains 10 parameters, including location coordinates of fault and depth (x, y,-d), length (along the strike), width (along the dip), dip and strike of the fault and three slip components [17]. We then simulated InSAR deformation through adjusting some uncertain fault geometry parameters by Okada formula and then project onto the radar LOS direction. The ground surface displacement derived from Okada formula are

compared to coseismic displacements obtained from InSAR, and parameters are re-estimated until the results from Okada formula closely resemble InSAR results. The Single-patch model yields a slip of 2.5 meters.

## 4. Inversion Analysis using Multi-patch Model

To refine the result of Single-patch model, the planar fault is divided into smaller rectangular areas, each of which may assume different slip values. This model provides more realistic values of slip than Single-patch. As for the Single-patch, it is started by dividing of the fault into a series of rectangular patches along the direction of strike and dip and then integrating half-space Green's functions over area of fault for unit slip of each patch. The observed deformation data have to resample to get a lower image resolution before inversion [18]. In this sense, we downsampled interferograms pixel by quad-tree subsampling to divide into successively smaller boxes until variance fall below a threshold. To characterize the error terms that is correlated spatially, we estimate covariance from non-deforming region.

After that, we then set up model fault and calculate LOS phase at quad-tree centres for 1 meter of strike-slip and dip-slip motion. To estimate slip on fault given InSAR data and variance-covariance matrix, Therefore, to fixed fault geometry for a linear problem, we set up design matrix A, in form: y = Ax, where y is vector of LOS observations and x is vector of model parameters as shown in Eq. (1) and (2) [19]. The outputs from the model are then be used as the parameter for Single-patch model which are earthquake epicenter (607516E, 2288195N), strike (N70E°), dip (86°), rake (0), length (24.31 kilometers), $M_w$ (6.7), and slip (2.5 meters).

$$y = Ax \tag{1}$$

$$[\,D_{insar}\_\mathrm{Los}] = [G_{SS}\;\; G_{ds}\;\; 1]\begin{bmatrix} ss \\ ds \\ offset \end{bmatrix} \tag{2}$$

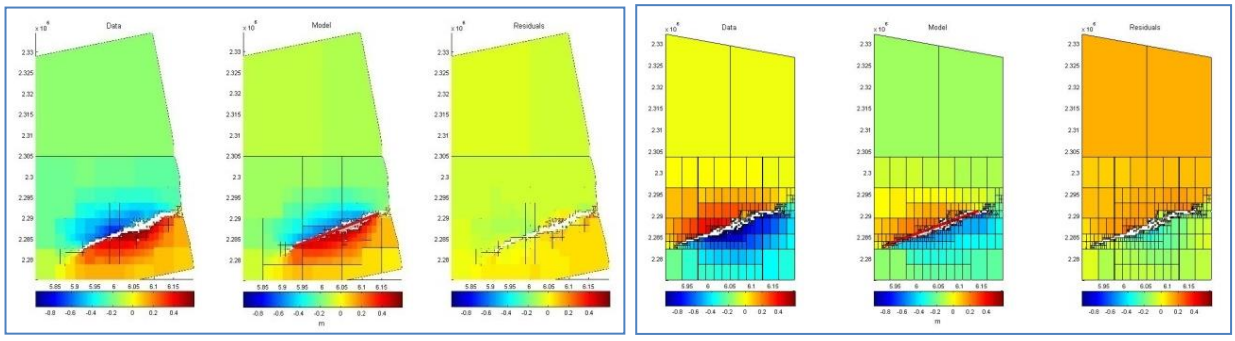


Fig. 4. Coseismic displacement in LOS direction of the ascending (left) and descending (right) path from downsampled interferogram, model and residual respectively.

Figure 4 shows the coseismic displacement from downsampled interferogram. The results from both InSAR and model are then compared, and we can find the ranges of residuals which describes the relation between the model prediction and the InSAR observation of two fault models. We found the difference in residuals in the descending (± 0.2 meters.) path which is larger than ascending path. It is important to note that the ascending path shows entirely satisfied results while the descending path contrary performance presents noticeably large residuals in particular parts which however do not have huge impact to the whole process.

For Multi-patch model, the slip on multiple fault patches is estimated. Since each fault patch is assumed to slip differently, we chose a 24 kilometers long fault plane and divided to 30 patches. We set up design matrix and weighted using least squares method. We assume that the Laplacians have a Gaussian distribution for additional smoothing constraint. The value of $\alpha^2$ is important because it is governed by the size of the scalar smoothing factor. The best-fit slip distribution depends on the size of the smoothing factor $\alpha^2$: high values lead to an over smooth solution with large misfit, low values result in smaller misfits, but oscillating slip distributions [19] as in Eq. (3).

DOI:10.4186/ej.2015.19.2.157

$$\begin{bmatrix} y \\ 0 \\ \vdots \\ 0 \end{bmatrix} = \begin{bmatrix} A & 1 \\ \alpha^2 L & 0 \quad 0 \\ 0 & \alpha^2 \; L0 \end{bmatrix} \begin{bmatrix} ss \\ ds \\ offset \end{bmatrix} \tag{3}$$

We subsequently plot a simulated interferogram for the values in x and fix geometry of fault and invert only for slip, which makes it a nonlinear problem compare to original interferogram. By minimizing the square misfit between the observed and predicted phase change nonlinear, Monte Carlo algorithm has been applied to sample the distribution in a representative way. We found that the slip from both model are maximum varied 0.27 meters. The 2.5 meters slip value from Single-patch model is used in coulomb stress change for slip distribution as shown in Fig. 5. The distributions of slip in each patch are shown in Table 2.

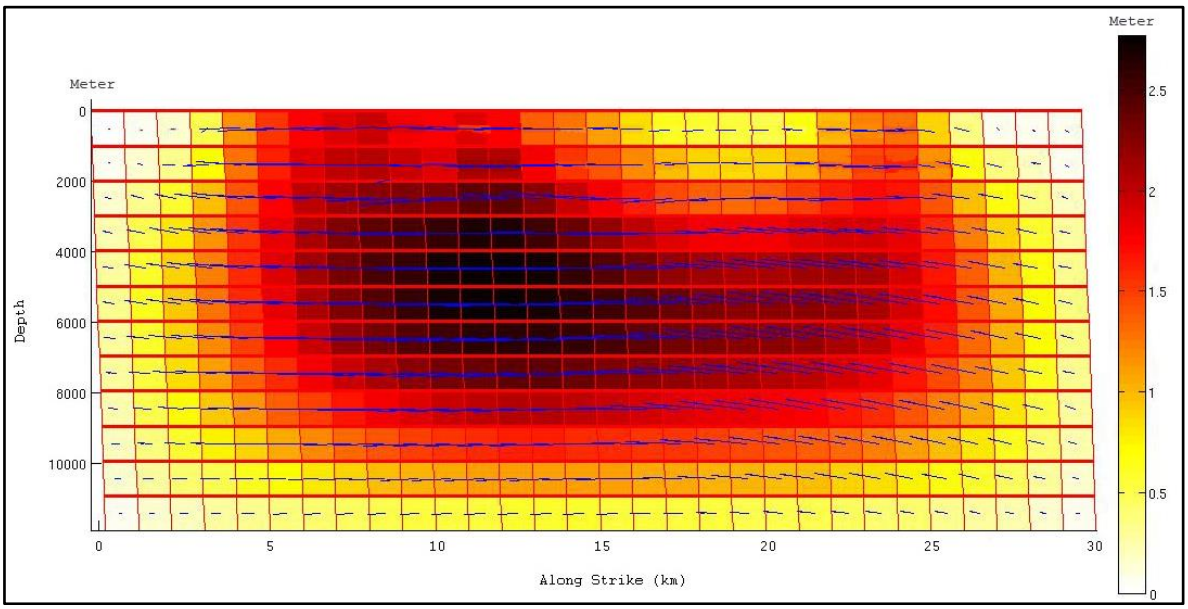


Fig. 5. Distribution of fault slip in Tarlay earthquake, maximum slip is 2.77 meters at depth 5-6 kilometers. Most of occurring is approximately 10 kilometers below surface.

Table 2. Distribution of fault slip from inversion analysis using multi-patch model as refer to Fig. 5.

| Dept (km.) \ Along Strike (km.) No. of Patch | 1 | 2 | 3 | 4 | 5 | 6 | 7 | 8 | 9 | 10 | 11 | 12 | 13 | 14 | 15 | 16 | 17 | 18 | 19 | 20 | 21 | 22 | 23 | 24 | 25 | 26 | 27 | 28 | 29 | 30 |
|---|---|---|---|---|---|---|---|---|---|---|---|---|---|---|---|---|---|---|---|---|---|---|---|---|---|---|---|---|---|---|
| 1 | 0.00 | 0.00 | 0.11 | 0.39 | 1.14 | 1.53 | 1.75 | 1.90 | 1.95 | 1.74 | 1.20 | 1.80 | 1.76 | 1.32 | 1.00 | 1.04 | 0.84 | 0.48 | 0.39 | 0.41 | 0.40 | 0.61 | 0.87 | 1.06 | 1.23 | 0.91 | 0.27 | 0.06 | 0.00 | 0.00 |
| 2 | 0.05 | 0.13 | 0.34 | 0.69 | 1.26 | 1.64 | 1.87 | 2.01 | 2.06 | 1.96 | 1.81 | 2.09 | 2.07 | 1.77 | 1.49 | 1.37 | 1.18 | 0.93 | 0.83 | 0.82 | 0.85 | 1.02 | 1.23 | 1.39 | 1.43 | 1.13 | 0.65 | 0.34 | 0.15 | 0.05 |
| 3 | 0.14 | 0.32 | 0.59 | 0.96 | 1.41 | 1.76 | 2.00 | 2.16 | 2.24 | 2.25 | 2.27 | 2.41 | 2.40 | 2.21 | 1.98 | 1.80 | 1.62 | 1.45 | 1.35 | 1.34 | 1.38 | 1.49 | 1.63 | 1.71 | 1.65 | 1.39 | 0.99 | 0.64 | 0.38 | 0.17 |
| 4 | 0.22 | 0.47 | 0.78 | 1.14 | 1.52 | 1.85 | 2.10 | 2.28 | 2.40 | 2.48 | 2.56 | 2.65 | 2.64 | 2.52 | 2.35 | 2.18 | 2.02 | 1.88 | 1.80 | 1.78 | 1.81 | 1.87 | 1.94 | 1.94 | 1.83 | 1.57 | 1.22 | 0.87 | 0.55 | 0.27 |
| 5 | 0.28 | 0.57 | 0.89 | 1.23 | 1.58 | 1.89 | 2.14 | 2.33 | 2.48 | 2.60 | 2.69 | 2.77 | 2.77 | 2.69 | 2.57 | 2.43 | 2.30 | 2.19 | 2.12 | 2.09 | 2.10 | 2.12 | 2.12 | 2.07 | 1.92 | 1.67 | 1.35 | 1.00 | 0.66 | 0.32 |
| 6 | 0.30 | 0.61 | 0.93 | 1.25 | 1.57 | 1.86 | 2.10 | 2.29 | 2.45 | 2.58 | 2.69 | 2.75 | 2.77 | 2.72 | 2.63 | 2.53 | 2.42 | 2.34 | 2.28 | 2.24 | 2.22 | 2.21 | 2.17 | 2.08 | 1.92 | 1.68 | 1.38 | 1.04 | 0.70 | 0.35 |
| 7 | 0.30 | 0.60 | 0.91 | 1.21 | 1.49 | 1.75 | 1.98 | 2.17 | 2.33 | 2.45 | 2.55 | 2.62 | 2.64 | 2.61 | 2.56 | 2.48 | 2.40 | 2.33 | 2.27 | 2.23 | 2.20 | 2.16 | 2.10 | 1.99 | 1.82 | 1.60 | 1.32 | 1.01 | 0.68 | 0.34 |
| 8 | 0.28 | 0.56 | 0.83 | 1.10 | 1.35 | 1.58 | 1.78 | 1.95 | 2.10 | 2.22 | 2.31 | 2.37 | 2.39 | 2.38 | 2.34 | 2.29 | 2.23 | 2.18 | 2.13 | 2.09 | 2.04 | 1.99 | 1.92 | 1.81 | 1.65 | 1.44 | 1.20 | 0.92 | 0.63 | 0.32 |
| 9 | 0.24 | 0.48 | 0.71 | 0.94 | 1.15 | 1.34 | 1.51 | 1.66 | 1.79 | 1.89 | 1.97 | 2.02 | 2.04 | 2.04 | 2.02 | 1.98 | 1.94 | 1.90 | 1.86 | 1.82 | 1.77 | 1.72 | 1.65 | 1.54 | 1.40 | 1.23 | 1.02 | 0.79 | 0.54 | 0.27 |
| 10 | 0.19 | 0.38 | 0.57 | 0.74 | 0.91 | 1.06 | 1.19 | 1.31 | 1.40 | 1.48 | 1.55 | 1.59 | 1.61 | 1.61 | 1.60 | 1.58 | 1.55 | 1.52 | 1.48 | 1.45 | 1.41 | 1.36 | 1.30 | 1.21 | 1.10 | 0.96 | 0.80 | 0.62 | 0.42 | 0.21 |
| 11 | 0.13 | 0.26 | 0.39 | 0.51 | 0.62 | 0.73 | 0.82 | 0.90 | 0.97 | 1.02 | 1.07 | 1.10 | 1.11 | 1.11 | 1.11 | 1.09 | 1.08 | 1.05 | 1.03 | 1.01 | 0.98 | 0.94 | 0.90 | 0.84 | 0.76 | 0.66 | 0.55 | 0.43 | 0.29 | 0.15 |
| 12 | 0.07 | 0.14 | 0.20 | 0.26 | 0.32 | 0.37 | 0.42 | 0.46 | 0.49 | 0.52 | 0.54 | 0.56 | 0.57 | 0.57 | 0.57 | 0.56 | 0.55 | 0.54 | 0.53 | 0.52 | 0.50 | 0.48 | 0.46 | 0.43 | 0.39 | 0.34 | 0.28 | 0.22 | 0.15 | 0.08 |

According to Fig. 5, the result displays the invert for the fault slip distribution along Tarlay earthquake. We divided 30 patches along strike (1 patch is approximately 1 kilometer) and 12 patches in down dip. The result from the model indicates that Nam Ma fault is characterized as a pure strike-slip type with a small dip-slip. The maximum slip is 2.77 meters in the depth 5-6 kilometers. The major group of slip rate locates between 3-8 kilometers depth in the middle and west of Nam Ma fault. The maximum number of slip near the surface is 1.95 meters (< 1 kilometer at deep) and less than the number of slip rate at 3-8 kilometers below surface.

We then use the slip from the top patch (at a depth from the surface about 1 kilometer) to compare with the values obtained from the field survey. The value from top patch is an indication of magnitude and direction of the fault closest to the actual terrain surface as shown in Fig. 6.

DOI:10.4186/ej.2015.19.2.157

## 5. Comparison of Slip Distribution with Field Data

Figure 6 reveals a field survey data after Tarlay earthquake Myint, et al. [20]; the yellow points in the image indicate the position of field survey in the areas. The yellow numbers in the image indicate the offset values in the areas. The total length of fault (red line in Fig. 6) is approximately 30 kilometers and the maximum offset value is 1.25 meters in the western of the fault. The graph below displayed a comparison between the slip obtained from field survey and the slip distribution using Multi-patch model. The comparison between those data is estimated base on coordinate information judgment as obtained from [20], so the starting point (first point) from field survey will begin at kilometer 10.

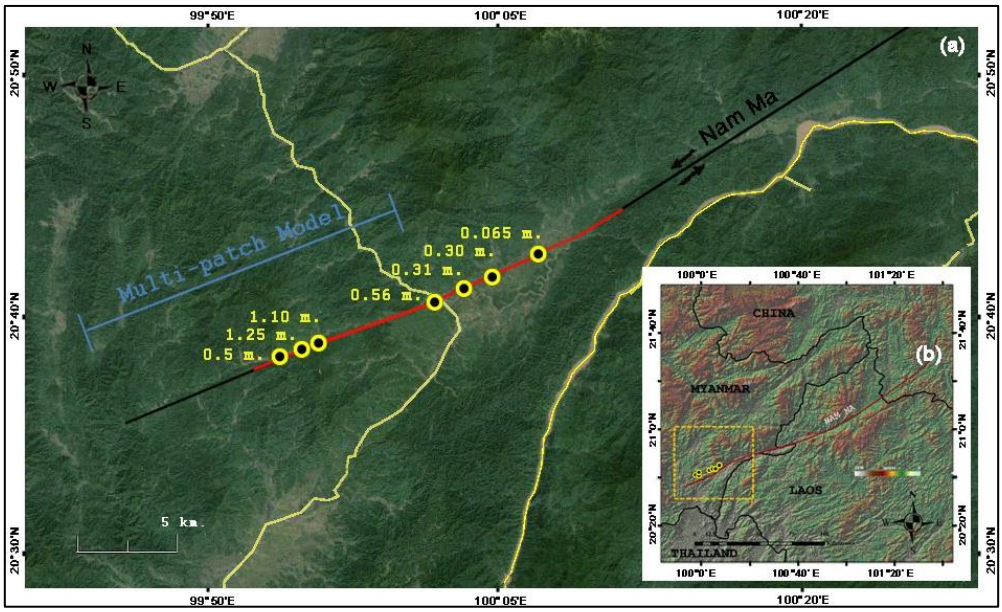


Fig. 6. Map shows the position of the field survey data in [20] on the west side of the Nam Ma fault. The blue line indicates the length of fault which is resulted from Multi-patch model analysis. The origins used in comparison between model analysis and field survey analysis are unequal.

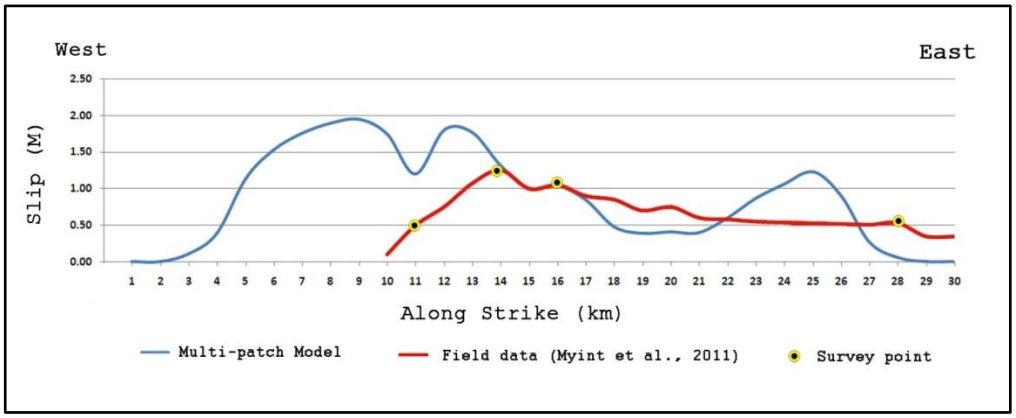


Fig. 7. The graph shows a comparison of the slip distribution. Red line is obtained from the field survey, yellow points indicate field survey locations [20], and the blue line is slip distribution of the results.

The blue line in Fig. 7 is the slip from Multi-patch model, and the red line is obtained from the field data within 20 kilometers. The result revealed that the slip from Multi-patch model is lower than field survey in kilometer 17-22 and 27 onwards. In kilometer 14 to 16, the slip from both approaches has almost the same. Refer to the field survey data from [6], this can be explained that the area is offset paddy field berm and the range of the offset field is highest. For the eastern end of the fault, slip will be gradually reduced due to the distance away from the epicenter. Thus, it can be concluded here that the main

DOI:10.4186/ej.2015.19.2.157

difference between model and field survey in this case are the physical geography in the area and the lack of coordinate information from the field data to make starting point difficult to adjust.

The difference between computed slips on the top patches and observed slip in the field could be resulted from three main factors. First, the filed-surveyed slips are measured on top soil, the depth of which over the below bedrock is unknown but could vary from few tens to hundreds meters. On the contrary, the computed slips are the values of the underneath rock which is not observable. Second, the precise coordinates of the locations of field-surveyed slips are not available to us. We could only best-guess the locations from various sources of maps, diagram and satellite images but it is likely that errors are large. Third, the Multi-patch solution from Laplacian smoothing explained in section 4 is not unique. There could be many slip distribution models that resulted in the same magnitude of this Tarlay earthquake. We choose the one that seems to agree most with the known mechanics of fault such as localization of large slips and slip directions do not deviate much from patch to patch. Nevertheless, with the currently available data, we cannot explain with certainty the large differences in the segment from kilometer 10-13 and from kilometer 24-26. On the other hand there is a well-agreed segment of kilometer 14-16 and another segment with relatively small differences from kilometer 16-22. Further work such as seismic slip inversion could provide independent validation of our result.

## 6. Coulomb Stress Change Computation

We use USGS Coulomb program 3.3 version to compute stress change in nearby faults [21]. The parameters of the ruptured segment of Nam Ma fault is obtained from Single-patch model. The faults included in this analysis are Mae Chan, Chiang San, Mae Lao, Mae Suai, Chiang Kham and Mae Ing.

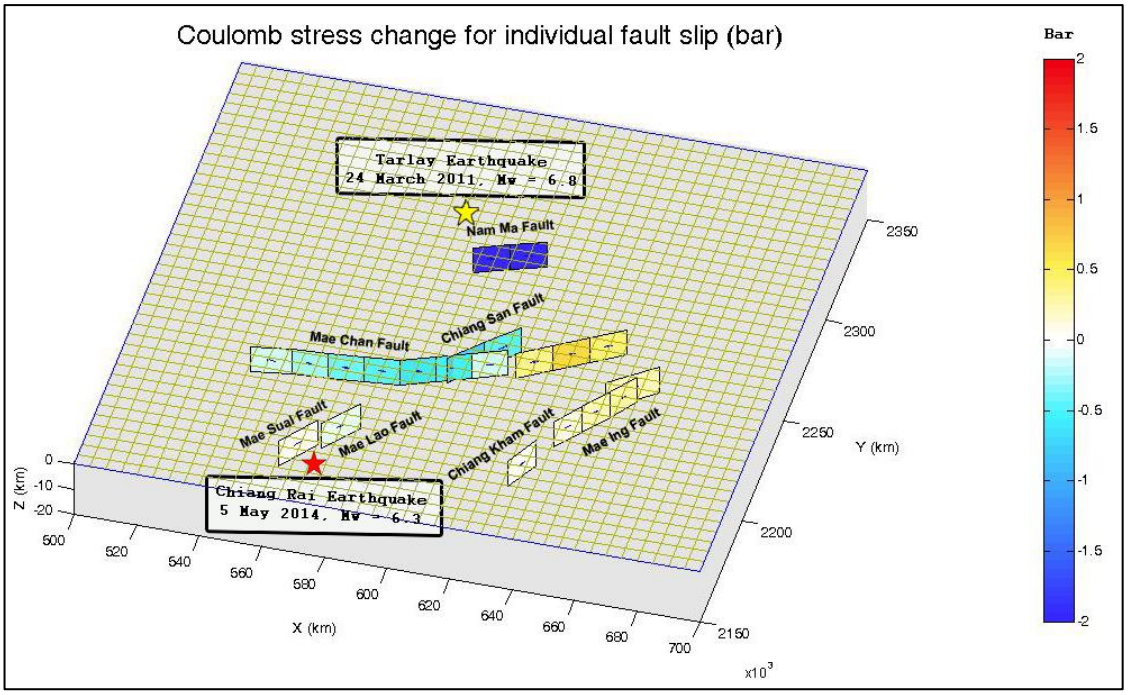


Fig. 8. Coulomb stress change result on Mae Chan and nearby fault in upper northern of Thailand after the Tarlay earthquake. Red star shows the epicenter of $M_w$=6.3 Chiang Rai earthquake, occurring on 5 May 2014.

As shown in Fig. 8, Nam Ma fault releases its stress during the earthquake, and the stress is re-distributed to surrounding area, especially near the Mae Chan fault slips. If we primarily consider Mae Chan fault, the east end of Mae Chan fault could be failure caused by the increasing of the stress as indicated in the maximum value of coulomb stress scale around 0.6 bar. At the same time, the west and middle of the fault are stress shadow zone. The others interesting faults are Chiang Kham and Mae Ing fault because the coulomb stress is increased in about 0.15 bar. For other faults, the remaining value of the stress is decreased, so this analytical result indicates that the eastern of Mae Chan, Mae Ing and Chiang Kham faults could have a high probability of seismic risk. After Tarlay earthquake about 3 years, the earthquake

occurred in Chiang Rai on 5th May, 2014 with $M_w$=6.3. Although the result from coulomb stress change in Mae Lao fault And Mae Suai fault was given to -0.15 bar which represent a reduction of stress, but this is just the risk assessment for the probability of the earthquake arise in the future. The data from Chiang Rai earthquake is the one to support that the faults in the upper north of Thailand have stress transfer, and it is interesting that the increasing chance of earthquake event in other faults of Thailand.

## 7. Time-series InSAR for Postseismic Deformation Detection

The postseismic investigation is performed by processing the 19 Radarsat-2 images (Beam type: F3N, Incidence angle: 42º) with Time-series InSAR analysis. Rational and details of each processing steps of this technique can be found in [22]. Acquisition date and baseline information of the images, acquired from June, 2011 till May, 2013 in ascending orbit covering the Mae Chan fault and Nam Ma fault area, are shown in Table 3. All images are co-registered to the master imagery of 20 March, 2012. The master image is chosen by maximizing (predicted) total coherence of the interferometric stack, based on the perpendicular baseline, temporal baseline, the mean Doppler centroid frequency difference and thermal noise [22].

Table 3. Acquisition and pairing details of Radarsat-2 images, ascending orbit.

| No. | Date | Perpendicular Baseline (Meter) | Temporal Baseline (Day) |
|---|---|---|---|
| 1 | 30 June 2011 | -132 | 264 |
| 2 | 24 July 2011 | -108 | 240 |
| 3 | 17 August 2011 | -30 | 216 |
| 4 | 4 October 2011 | -57 | 168 |
| 5 | 28 October 2011 | 197 | 144 |
| 6 | 21 November 2011 | 101 | 120 |
| 7 | 15 December 2011 | 112 | 96 |
| 8 | 8 January 2012 | -1026 | 72 |
| 9 | 1 February 2012 | -129 | 48 |
| 10 | 25 February 2012 | -90 | 24 |
| 11 | 20 March 2012 | 0 | 0 |
| 12 | 13 April 2012 | 158 | 24 |
| 13 | 7 May 2012 | -576 | 48 |
| 14 | 31 May 2012 | 155 | 72 |
| 15 | 24 July 2012 | 290 | 96 |
| 16 | 19 February 2013 | -37 | 240 |
| 17 | 15 March 2013 | -86 | 264 |
| 18 | 8 April 2013 | -100 | 288 |
| 19 | 26 May 2013 | 165 | 312 |

We employ StaMPS/MTI software package to analyze a suite of Radarsat-2 images with a variant of Time-series InSAR technique known as Persistent Scatterer (PS) method. Figure 9 illustrates Time-series InSAR processing flow. The initial part of the process is the generation of interferograms using DORIS software [23]. In this part, the 3 arc-second (90 meter) resolution of SRTM DEM was used to remove topographic phase. All interferograms were simultaneously processed iteratively, using only pixels whose phases are considered stable. Then, phase stability which is contained in each pixel was initially rejected based on their amplitude characteristics. For the PS pixel selection [24], we converted all data into a preferred format for PS processing. Next, phase noise which exists in each candidate pixel of every interferogram was estimated and selected based on their stochastic characteristics. After that, the pixels selection in the previous step were weeded and corrected for spatially-uncorrelated look angle error and master atmosphere and orbit error. Values of spatially-correlated look angle error which occurs from DEM and orbital error were calculated and eliminated using measure of the phase noise level equation [24]. The phase change is then unwrapped and then each PS point is assigned with the velocity or rate of phase change resulted from regression in time.

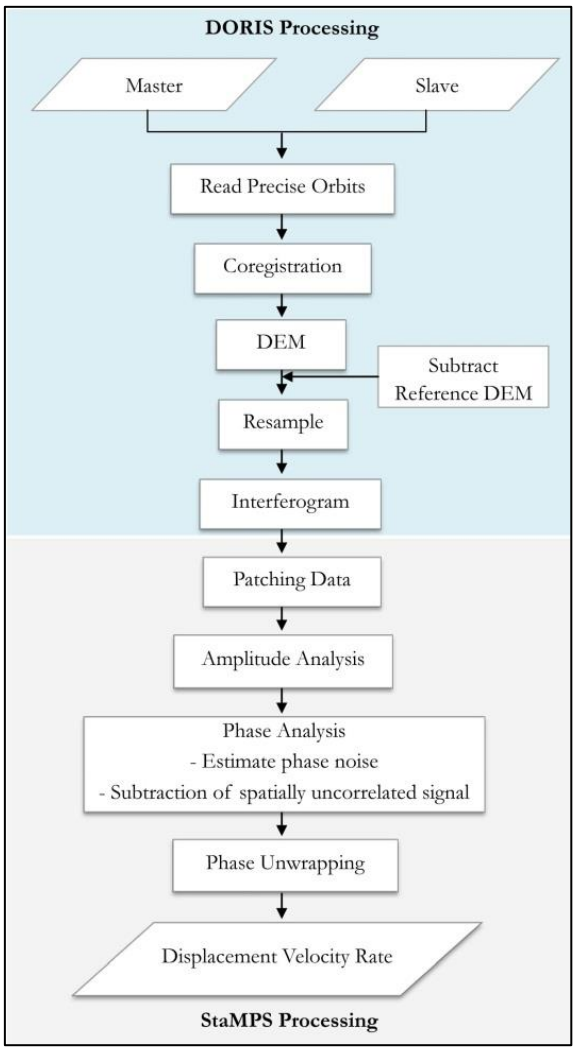


Fig. 9. Time-series InSAR processing flow using DORIS and StaMPS software.

The result from PS technique reveals the postseismic deformation of Tarlay earthquake spanning approximately two years. There are more than 147,000 PS points of ascending path with LOS displacement rate between -24.4 to 34.5 millimeters per year as shown in Fig. 10(a). The results show the positive range change (blue) i.e. moving away from the sensor in the southern part of Nam Ma fault while the northern show negative range change (red) meaning moving toward the sensor direction. The result was consistent with left-lateral fault movement. The white dash line shows an imaginary transect across the Nam Ma fault line. Figure 10(b) shows profile of this transect. It can be seen that the LOS velocities are symmetrical across the fault. The displacement pattern is consistent with Reid's elastic rebound model [8–9] in postseismic phase.

DOI:10.4186/ej.2015.19.2.157

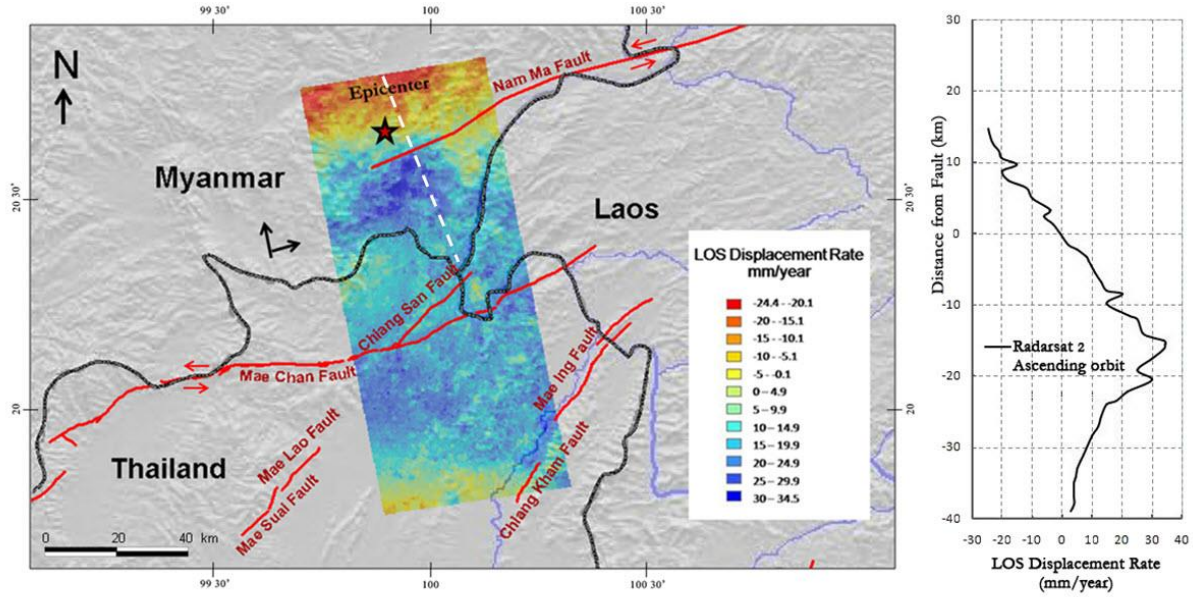


Fig. 10 (a) Displacement rate (milimeter/year) in Nam Ma and Mae Chan fault region from Time-series InSAR analysis of a suite of 19 Radarsat-2 imageries from June 2011 to May 2013. Dark arrows show direction of Radarsat-2 trajectory and its LOS. Negative range changes (red) were detected in the area north of Nam Ma fault and positive range change (blue) in the south of the fault. White dash line shows an imaginary transect crossing Nam Ma fault line; (b) the profile of the transect shown in (a).

## 8. Conclusion

The InSAR coseismic motion is used in the inversion analysis to determine Nam Ma fault parameters. The Single-patch model yields a coseismic slip of 2.5 m. From the Multi-patch model, the maximum slip in top patch is 1.95 meters at depth of about 1 kilometers. When compare with the values obtained from field survey, we found rather large differences in western segment while the surface slip are almost the same in kilometres 14-16.

The result from the simple fault plane model is used in the Coulomb stress change computation in nearby faults. It reveals that the stress increases 0.6 bar in the east end of the Mae Chan, and 0.15 bar in Mae Ing fault and Chiang Kham fault. The remaining faults indicate as a stress shadow.

By using the slip rate in the interseismic stage of Nam Ma fault from [4] the values of which are between 0.6-2.4 millimetres per year with the slip of 2.5 m from Single-patch model, the recurrence period is approximated to be between 1,040-4,160 years. If we assume that earthquake is characterized by average slip of 1.36 m from multi-patch model, it yields recurrence period of approximately 560–2,260 years.

Radarsat-2 images are used to detect postseismic motion occurred in the past 2 years after Tarlay earthquake. The analytical result reveals that the LOS displacement is up to 3.45 centimeters per year with the highest deformation locating 10-20 kilometres. Continuing data is required in order to determine the interseismic rate of this segment of Nam Ma fault which would enable the computation of a more reliable recurrence period.

The recent Chiang Rai earthquake occurring on 5 May 2014 $M_w$=6.3 exposed the seismic risk of northern Thailand region. The earthquake epicenter is located at the depth of about 7.4 kilometers on Mae Suai fault [25]. Although our Coulomb stress change result does not show stress increase on Mae Suai fault, it becomes imperative to monitor all nearby faults such as Phayao and Chiang Mai fault since the orientation of these faults could be in favour of receiving stress increase from Chiang Rai earthquake and therefore result in higher probability of large earthquake occurring in the near future.

## Acknowledgments

The authors thank the Department of Survey Engineering and Chulalongkorn University for facilities support. The Radarsat-2 SAR data used in this work are supported by Geo-Informatics and Space Technology Development Agency (GISTDA) with cooperating from Canadian Space Agency (CSA) and MacDonald, Dettwiler and Associates Ltd. (MDA), all of which we would like to thank. We would like to express our appreciation to Prof. Dr. Andy Hooper, of the School of Earth and Environment, Faculty of Environment, University of Leeds, UK, for his training and support. Finally, our sincere thanks to the reviewers whose valuable comments have led to a significant improvement of this paper.

## References

[1] J. McCaughey and P. Tapponnier. (2011). *Myanmar earthquake of March 24, 2011 - Magnitude 6.8* [Online]. Available: http://www.earthobservatory.sg/media/news-and-features/295-myanmar-earthquake-of-march-24th-magnitude-68.html

[2] I. Trisirisatayawong, A. Hooper and A. Aobpaet, "Co-seismic displacement of 24-March 2011 $M_w$ 6.8 Mong Hpayak Earthquake, Myanmar," in Proceedings *FRINGE Workshop ESA SP (Vol. 697)*., Frascati, Italy, 2011.

[3] T. Ornthammarath, "A note on the strong ground motion recorded during the $M_w$ 6.8 earthquake in Myanmar on 24 March 2011," *Bull Earthquake Eng*, vol. 11, no. 1, pp. 241–254, Sep, 2013.

[4] R. Lacassin, A. Replumaz, and P. H. Leloup, "Hairpin river loop and slip sense inversion on SE-Asian strike-slip faults," *Geology*, vol. 26, no. 8, pp. 703–706, Aug, 1998.

[5] Y. Wang, "Earthquake geology of Myanmar," Ph.D. thesis, California Institute of Technology, 2013.

[6] S. T. Tun, S. N. Khaing, Y. Wang, M. Thant, N. Htay, Y. Myo, M. Htwe, T. Myint, and K. Sieh, "Surface ruptures of the 2011 Tarlay earthquake and their relationship to the active tectonics of eastern Myanmar," submitted for publication.

[7] Y. Wang, Y. N. Lin, M. Simons, and S. T. Tun, "Shallow rupture of the 2011 Tarlay earthquake (Mw 6.8) eastern Myanmar," *Bull. Seismol. Soc. Am.*, vol. 104, no. 6, pp. 2904–2914, Dec, 2014.

[8] W. Thatcher, "The earthquake cycle and its role in the long-term deformation of continental lithosphere," *Annali Di Geofisica*, vol. 36, no. 2, pp. 13–24, May, 1993.

[9] T. J. Wright, "Remote monitoring of the earthquake cycle using satellite radar interferometry," *Phil. Trans. R. Soc. Lond. A*, vol. 360, no. 1801, pp. 2873–2888, Dec, 2002.

[10] M. Chini, S. Atzori, E. Trasatti, C. Bignami, C. Kyriakopoulos, C. Tolomei, and S. Stramondo, "The May 12, 2008, (Mw 7.9) Sichuan Earthquake (China): Multiframe ALOS-PALSAR DInSAR analysis of coseismic deformation," *IEEE Geoscience and Remote Sensing Letters*, vol. 7, no. 2, pp. 266–270, Apr, 2010.

[11] M. de Michele, D. Raucoules, C. Lasserre, E. Pathier, Y. Klinger, J. Van der Woerd, J. de Sigoyer, and X. W. Xu, "The Mw 7.9, 12 May 2008 Sichuan earthquake rupture measured by sub-pixel correlation of ALOS PALSAR amplitude images," *Earth Planets Space*, vol. 62, no. 11, pp. 875–879, Nov, 2010.

[12] E. J. Fielding, A. Sladen, Z. Li, J. P. Avouac, R. Bürgmann, and I. Ryder, "inematic fault slip evolution source models of the 2008 Mw 7.9 Wenchuan earthquake in China from SAR interferometry, GPS and teleseismic analysis and implications for Longmen Shan tectonics," *Geophys. J. Int.*, vol. 194, no. 2, pp. 1138–1166, Aug, 2013.

[13] M. Furuya, Y. Kobayashi, T. Takada, and M. Murakami, "Fault source modeling of the 2008 Wenchuan earthquake based on ALOS/PALSAR Data," *Bull. Seismol. Soc. Am.*, vol. 100, no. 5B, pp. 2750–2766, Nov, 2010.

[14] S. Stramondo, M. Chini, C. Bignami, S. Salvi, and S. Atzori, "X-, C-, and L-Band DInSAR Investigation of the April 6, 2009, Abruzzi Earthquake," *IEEE Geoscience and Remote Sensing Letters*, vol. 8, no. 1, pp. 49–53, Jan, 2011.

[15] J. Beavan, M. Motagh, E. J. Fielding, N. Donnelly, and D. Collett, "Fault slip models of the 2010–2011 Canterbury, New Zealand, earthquakes from geodetic data, and observations of post-seismic ground deformation," *New. Zeal. J. Geol. Geop.*, vol. 55, no. 3, Aug, 2012.

[16] J.R . Elliott, E. K. Nissen, P. C. England, J. A. Jackson, S. Lamb, Z. Li, M. Oehlers, and B. Parsons, "Slip in the 2010–2011 Canterbury earthquakes, New Zealand," *J. Geophys. Res.*, vol. 117, no. B3, Mar, 2012.

[17] Y. Okada, "Surface deformation due to shear and tensile faults in a half space," *Bull. Seismol. Soc. Am.,* vol. 75, no. 4, pp. 1135–1154, Aug, 1985.
[18] X. Shan, G. Zhang, C. Wang, C. Qua, X. Song, G. Zhang, and L. Guo, "Source characteristics of the Yutian earthquake in 2008 from inversion of the co-seismic deformation field mapped by InSAR," *J. Asian. Earth. Sci.,* vol. 40, no. 4, pp. 935–942, June, 2011.
[19] A. Hooper, "Inversion of InSAR data for the estimation of movement on faults," in *GEO2TECDI-SONG InSAR Workshop*, Bangkok, Thailand, 2011.
[20] U. T. Myint, U. S. T. Tun, U. S. NgweKhine, U. S. Htwezaw, M. Thant, and Y. M. M. Htwe, "Myanmar Earthquake Committee Tarlay Earthquake (6.8 Magnitude, 24 March 2011)," Survey trip Pre-report.
[21] S. Toda, R. S. Stein, V. Sevilgen, and J. Lin. (2011). Coulomb 3.3 graphic-rich deformation and stress-change software for earthquake, tectonic, and volcano research and teaching user guide. [Online]. Available: http://usgsprojects.org/coulomb/Coulomb33of2011-1060.pdf
[22] A. Hooper, P. Segall, and H. Zebker, "Persistent scatterer interferometric synthetic aperture radar for crustal deformation analysis, with application to Volcáno Alcedo, Galapagos," *J. of Geophys. Res.: Solid Earth*, vol. 112, no. B07407, Jul, 2007.
[23] Delft University of Technology, *DORIS Delft Object-oriented Radar Interferometric Software User's Manual and Technical Documentation*. [Online]. Available: http://doris.tudelft.nl/software/doris_v4.02.pdf
[24] A. Hooper, "Satellite radar interferometry: Methodology, quality control and application development," in *Presentation of InSAR Workshop*, Chulalongkorn University, Bangkok, Thailand, Mar. 23–27, 2009.
[25] Seismological Bureau of Thailand. (2014). *Local Earthquake* [Online]. Available: http://www.seismology.tmd.go.th/inside-info.html?earthquake=2085